

Push–pull type manganese(III)corroles: Synthesis, electronic structures and tunable interactions with ctDNA

Xu Liang,^{a,b,*} Junjia Fang,^a Minzhi Li,^a Qiuyun Chen,^a John Mack,^{c,*[◇]}
Nthabeleng Molupe,^c Tebello Nyokong^{c[◇]} and Weihua Zhu^{a,*}

^a School of Chemistry and Chemical Engineering, Jiangsu University, Zhenjiang 212013, P. R. China

^b State Key Laboratory of Coordination Chemistry, Nanjing University, Nanjing 210000, P. R. China

^c Centre for Nanotechnology Innovation, Department of Chemistry, Rhodes University, Grahamstown 6140, South Africa

Received 21 October 2017

Accepted 3 December 2017

ABSTRACT: The synthesis of three low symmetry A₂B type Mn(III)triarylcorroles with *meso*-aryl substituents that provide push–pull electron-donating and -withdrawing properties is reported. An analysis of the structure-property relationships for the optical and redox properties has been carried out through a comparison with the results of theoretical calculations. The results demonstrate that A₂B type Mn(III)triarylcorroles interact strongly with cell-free circulating tumor deoxyribonucleic acid (ctDNA) in solution, and that the interaction constants are enhanced when a stronger electron-donating substituent is introduced at the 10-position of the *meso*-triarylcorrole ligand.

KEYWORDS: Mn(III)corrole, DNA interaction, electronic structure, TDDFT calculation.

INTRODUCTION

Corroles are structural analogs of porphyrins that have a direct pyrrole–pyrrole bond and an extra NH proton in their inner core, which are perhaps best known in a manner that results in lower molecular symmetry and more intense absorption in the longer wavelength portion of the visible region [1, 2]. Corrole chemistry has inspired a wide range of applications including organic solar cells, photodynamic therapy, heat absorbers, bio-imaging and organic catalysis [3–8]. In recent decades, there has been a strong research focus on the use of corroles as functional ligands, largely due to their ability to stabilize higher oxidation states of coordinated metal. Manganese corroles have received considerable attention in this regard, since the 3d⁵ configuration of the Mn(II) ion readily loses electrons to form stable Mn(III), Mn(IV) and Mn(V)corrole structures, which exhibit no

fluorescence because of low-lying metal-to-ligand charge transfer (MLCT) states [9–11]. We have recently reported the properties of several metal triarylcorroles with push–pull A₂B substitution patterns with different *meso*-aryl substituents at the 5,15-(A₂) and 10-(B) positions [12]. The push–pull strategy involves the introduction of both electron-donating (push) and withdrawing (pull) substituents to effectively stabilize the LUMO orbitals and destabilize the HOMO orbitals, and this provides one of the most effective strategies for modulating the electronic structures of porphyrinoid π -systems. Large shifts are often observed in the wavelengths of the main spectral bands and in the redox potentials that can be readily rationalized through a consideration of how the alignments of the angular nodal patterns of the frontier π -MOs influence the effect of introducing the push–pull substituents [13, 14].

DNA carries the genetic instructions used in the growth, development, functioning and reproduction of living organisms and most viruses [15, 16]. The interactions between porphyrinoid chromophores and DNA by an outside binding mode have not been studied in depth. Several studies have shown, however, that porphyrinoids can interact with DNA. This approach can be used for

[◇] SPP full member in good standing

*Correspondence to: Xu Liang, email: liangxu@ujs.edu.cn, tel: & fax: +86 511-8879-1928; Weihua Zhu, email: sayman@ujs.edu.cn, tel: & fax: +86 511-8879-1928; John Mack, email: j.mack@ru.ac.za, fax: +27 46-622-5109.

tumor detection and targeting drug delivery *in vivo*, leading to tumor cell death without damage to normal tissue. According to previous studies, cationic metalloporphyrins can interact with DNA and induce and then stabilize the formation of G-quadruplex structures [17, 18]. It has previously been reported that the introduction of high-valence metal centers, such as Mn(III), Fe(III) and P(V) [19–22], can enhance the electronic attraction between the metalloporphyrin and DNA. The push–pull substitution strategy results in strong intramolecular charge transfer and this provides a new approach for studying the interaction between DNA and non-cationic metalloporphyrin, which is advantageous since the synthesis and purification of cationic metalloporphyrins is difficult to achieve. In this study, the synthesis, optical spectroscopy, electrochemistry, and TD-DFT calculations of a series of push–pull Mn(III) triarylporphyrins (**3a–3c**) is reported (Scheme 1) along with their interaction properties with cell-free circulating tumor deoxyribonucleic acid (ctDNA) in aqueous solution.

EXPERIMENTAL

Chemicals

The reagents and solvents that were used were of reagent grade and, except where noted, were used without further purification. Cyclic voltammetry measurements were carried out in a three-electrode cell using a Chi-730D electrochemistry station. A glassy carbon disk electrode was used as the working electrode, and the counter and reference electrodes were platinum mesh and a Ag/AgCl electrode, respectively. Magnetic circular dichroism (MCD) spectra were recorded on a JASCO J-815 spectrodichrometer equipped with a JASCO permanent magnet, which produces magnetic fields of up to 1.60 Tesla with both parallel and antiparallel fields. The MCD sign and Faraday term conventions of Piepho and Schatz are used throughout [23–25].

Computational methods

The Gaussian 09 software package [26] was used to carry out DFT geometry optimizations for **3a–3c** and

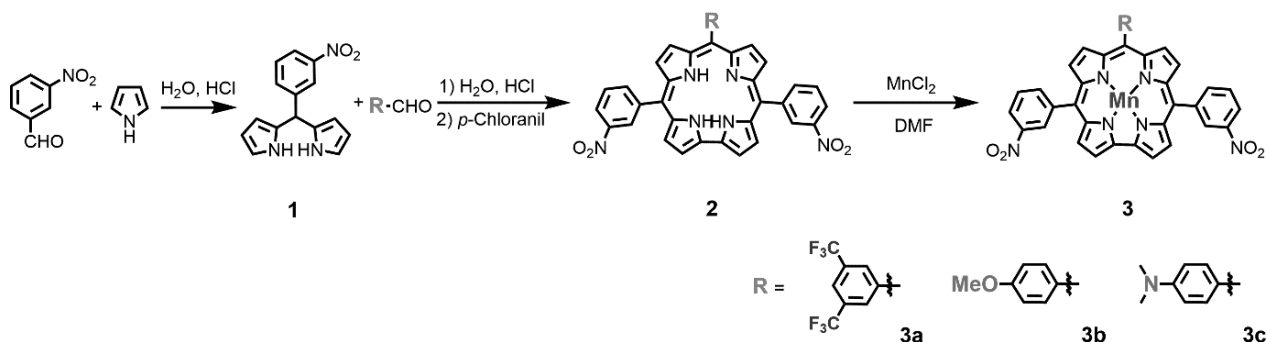
a model complex with a phenyl substituent as the A₂ *meso*-phenyl positions by using the B3LYP functional with 6-31G(d) basis sets. TD-DFT calculations were carried out in a similar manner with the CAM-B3LYP functional, since its long-range correction is known to provide more accurate predictions in the context of porphyrinoids with closed shell electronic configurations for the energies of transitions with significant charge transfer character [27, 28].

Sample preparation for DNA interaction

Electronic absorption spectroscopy is one of the most useful techniques for DNA binding studies [29, 30]. All of the experiments involving the interaction of **3a–3c** with ctDNA were conducted in buffer solution (50 mM NaCl, 5 mM tris-HCl, pH = 7.1) at room temperature. A solution of ctDNA in tris-HCl buffer solution gave ratios of UV absorbance at 260 and 280 nm of *ca.* 1.9, indicating that the DNA was sufficiently free of protein. The DNA concentration was determined by absorption spectroscopy using a molar absorption coefficient (6600 M·cm⁻¹) at 260 nm. Absorption titration measurements were carried out by varying the concentration of ctDNA-buffer solution upon addition of 50 μL of a 1 × 10⁻² M DMSO solutions of **3a–3c** and keeping a fixed complex concentration in tris-HCl buffer (pH = 7.11). For fluorescence quenching experiments, the ctDNA was pretreated with ethidium bromide (EB) for 30 min and **3a–3c** were then added to this mixture so their effect on the emission intensity could be measured at different temperatures. The quenching properties of the DNA complex in the presence of EB was analyzed by using the Stern–Volmer equation.

Synthesis of 5,15-(*m*-nitrophenyl)-10-(3,5-bis-trifluoromethylphenyl)Mn(III)corrole **3a**

Synthesis and purification of 5-(3-nitrophenyl)-dipyrromethane were carried out according to literature procedures [12, 31] to provide a precursor to form A₂B type triarylporphyrins. 5-(3-Nitrophenyl)-dipyrromethane (0.535 g, 2.0 mmol) and 3,5-bis-trifluoromethylbenzaldehyde (242 mg, 1.0 mmol) were dissolved in a mixture



Scheme 1. Synthesis of Mn(III)corroles **3a–3c**

of methanol (50 mL) and water (47.5 mL). 2.5 mL of concentrated hydrochloric acid was slowly added and the mixture was stirred at room temperature for 1 h under N_2 . The solid state compound was collected after filtration, and dissolved in $CHCl_3$. The organic phase was washed by $NaHCO_3$ aqueous solution, distilled water and dried with anhydrous $NaSO_4$. After removal of the solvent by rotary evaporation, the residue was dissolved in 20 mL of CH_2Cl_2 and chloranil (0.74 g, 3.0 mmol) and the mixture was heated at $50^\circ C$ for 3 h with progress monitored by TLC plate. After purification by silica gel column chromatography using CH_2Cl_2 /hexane (4:1) as the eluent, finally the H_3 -5,15-(3-nitrophenyl)-10-(3,5-bis-trifluoromethylphenyl)corrole **2a** was obtained by recrystallization from CH_2Cl_2 and hexane as a deep-violet solid in 12.1% yield (0.0748 g). The free base 5,15-(*m*-nitrophenyl)-10-(3,5-bis-trifluoromethyl-phenyl)corrole **2a** (0.0350 g, 0.05 mmol) and $MnCl_2$ (0.0623 g, 0.25 mmol; 5.0 eq) were dissolved in 5 mL DMF and stirred at $120^\circ C$ for 1 h. After removal of the solvent, purification by Al_2O_3 gel (CH_2Cl_2 :hexane = 2:1; v/v) gave the target compound **3a** in 90.2% yield (0.0281 g). MALDI-TOF-MS: $m/z = 804.96$ (Calcd. $[M]^+ = 804.53$). Elemental analysis: Found, C, 58.13; H, 2.45; N, 10.52; O, 7.99 (Calculated, C, 58.22; H, 2.38; N, 10.45; O, 7.95).

Synthesis of 5,15-(*m*-nitrophenyl)-10-(*p*-methoxyphenyl)Mn(III)corrole **3b**

The general synthetic procedure is similar to that of **3a**, but 5,15-(*m*-nitrophenyl)-10-(*p*-methoxyphenyl) corrole **2b** was used instead. The target compound **3b** was obtained in a 90.0% yield (0.0243 g). MALDI-TOF-MS: $m/z =$

699.22 (Calcd. $[M]^+ = 698.56$); Elemental analysis: Found, C, 65.44; H, 3.12; N, 12.36; O, 11.21 (Calculated, C, 65.34; H, 3.32; N, 12.03; O, 11.45).

Synthesis of 5,15-(*m*-nitrophenyl)-10-(*p*-*N,N'*-dimethylaminophenyl)Mn(III)corrole **3c**

The general synthetic procedure was similar with **3a**, but 5,15-(*m*-nitrophenyl)-10-(*p*-*N,N'*-dimethylaminophenyl) corrole **2c** was used instead. The target compound **3c** was obtained in a 63.2% yield (0.0173 g). MALDI-TOF-MS: $m/z = 711.99$ (calcd. $[M]^+ = 711.61$); Elemental analysis: Found, C, 65.76; H, 3.55; N, 13.79; O, 8.95 (Calculated, C, 65.83; H, 3.68; N, 13.78; O, 8.99).

RESULTS AND DISCUSSION

Synthesis and characterization

Free base corrole compounds (**2a–2c**) were synthesized from a reaction of dipyrromethane **1** and the appropriate aryl-aldehyde (Scheme 1) according to the literature procedures. Mn(III)corroles (**3a–3c**) were then synthesized by a metalation reaction of **2a–2c**, and were purified by Al_2O_3 gel column chromatography. The MALDI-TOF MS data for **3a** revealed an intense parent peak at 804.96 (calcd. $[M]^+ = 804.53$), providing direct evidence that the 5,15-(*m*-nitrophenyl)-10-(3,5-bis-trifluoromethyl-phenyl)Mn(III)corrole **3a** was successfully prepared. Similar parent peaks were also observed for **3b** and **3c**. Elemental analyses provided further evidence that the structures are consistent with those predicted on the basis of MS data.

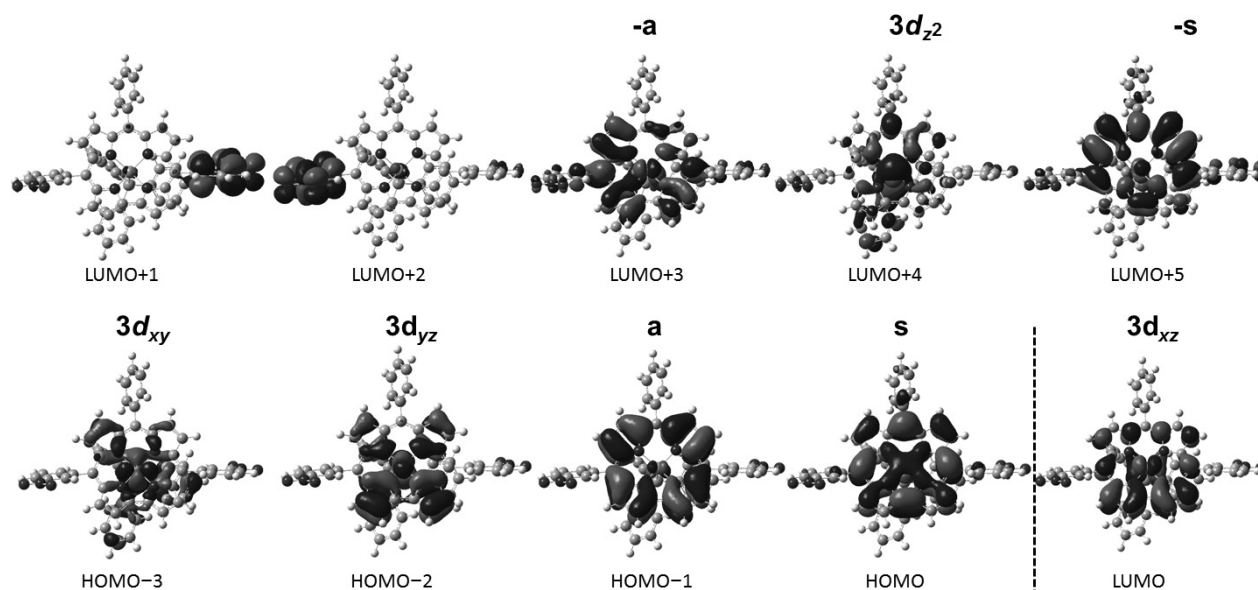


Fig. 1. The nodal patterns of a model complex with a phenyl ring at the B *meso*-aryl position (–H) at the CAM-B3LYP/6-31G(d) level of theory

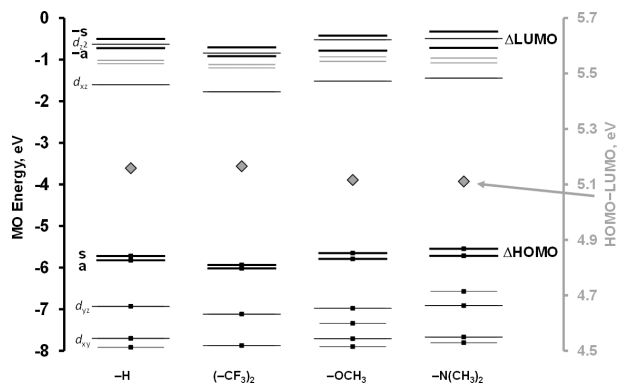


Fig. 2. The predicted MO energies for **3a–3c** and a model complex with a phenyl ring at the B *meso*-aryl position (**-H**) at the CAM-B3LYP/6-31G(d) level of theory. Occupied MOs are highlighted with small black squares. Gray diamonds are used to denote average HOMO–LUMO gap values for the **a**, **s**, **-a** and **-s** MOs that are associated with the corrole ligand and are plotted against a secondary axis. The **a**, **s**, **-a** and **-s** MOs are highlighted with thick black lines. Gray and longer black lines are used to denote MOs that are localized primarily on the A_2 position *meso*-aryl rings and the $3d$ orbitals of the Mn(III) ion, respectively

Optical spectra and TD-DFT calculations

The electronic structures and optical spectra of porphyrinoids can be readily rationalized by using Gouterman's 4-orbital model [32] and Michl's perimeter model [33–36]. The electronic structures and optical properties of corroles are reasonably similar to those of porphyrins [37]. The π -MOs associated with the 15 atom 18 π -electron inner ligand perimeter are arranged in an $M_L = 0, \pm 1, \pm 2, \pm 3, \pm 4, \pm 5, \pm 6, \pm 7$ sequence in ascending energy terms that is determined by the angular nodal properties. Since the HOMO and LUMO have M_L values of ± 4 and ± 5 , respectively, Gouterman's 4-orbital model predicts the presence of an allowed B transition ($\Delta M_L = \pm 1$) at high energy and a forbidden Q transition ($\Delta M_L = \pm 9$) at low energy for porphyrins and

their analogs such as corroles. Michl [33–36] referred to the π -MOs that are derived from the HOMO and LUMO of the parent perimeter as the **a** and **-a** MOs, respectively, if angular nodal planes lie on the y -axis, or as the **s** and **-s** MOs for the corresponding MOs that have significant MO coefficients on the y -axis (Fig. 1). In marked contrast with what is the case with free base corroles [3], the **a**, **s**, **-a** and **-s** MOs do not form the four frontier π -MOs in the TD-DFT calculations for **3a–3c** and there is significant mixing with close lying $3d$ orbitals of the Mn(III) ion (Fig. 1). The LUMOs are consistently predicted to be associated primarily with the $3d_{xz}$ orbital of the central metal ion (Figs 1 and 2) and the LUMO+1, LUMO+2 and LUMO+4 are associated primarily with the electron withdrawing NO_2 groups at the A_2 *meso*-positions and the $3d_{z^2}$ orbital of the central metal ion. The LUMO+3 and LUMO+5 are the **-a** and **-s** MOs, respectively, while in contrast, the **a** and **s** MOs consistently correspond to the HOMO–1 and HOMO. This means that the complexes are expected to undergo reduction initially at the metal center rather than on the corrole ligand.

A comparison with TD-DFT calculations demonstrates that the intense bands at around 420 nm and the shoulder of absorbance to high energy in the spectra of **3a–3c** (Figs 3 and 4 and Table 1) can be readily assigned to the B transitions. Further evidence can be derived for the MCD spectra, since there is an intense pair of oppositely-signed Faraday \mathcal{F}_0 terms in the MCD spectra (Fig. 1). The analysis of the weaker bands at lower energy in the visible region and near-infrared (500–800 nm) is complicated by the presence of ligand-to-metal charge transfer (LMCT) bands (Fig. 4), since the LUMO is predicted to be associated primarily with the $3d_{xz}$ orbital of the central metal ion (Figs 1 and 2). Regular Mn(III)-*meso*-triphenyl-corroles have weaker bands that lie at *ca.* 640 nm, and **3a** has similar spectral properties in this regard. The coupled pairs of oppositely-signed Faraday \mathcal{F}_0 terms in the 550–600 nm region of the MCD spectra of **3a–3c** can be assigned to the Q transition (Fig. 3), while

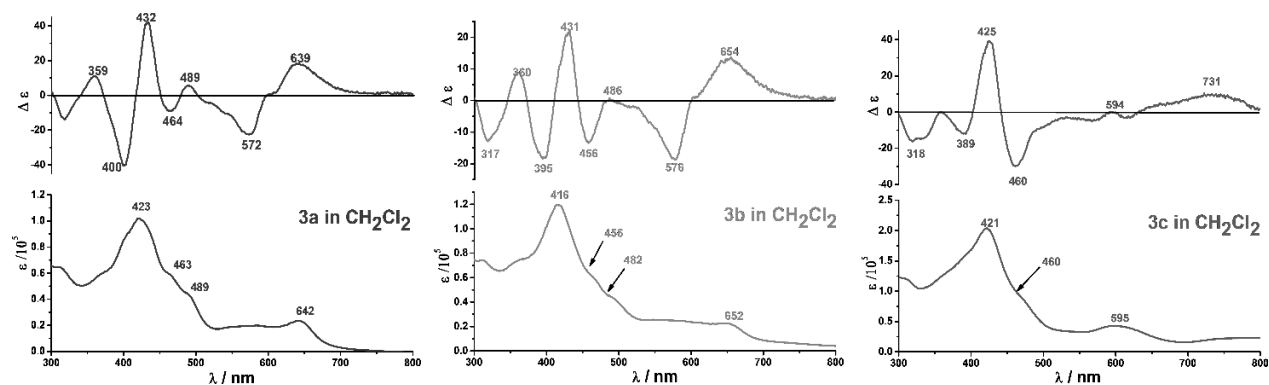


Fig. 3. Magnetic circular dichroism (MCD) and UV-visible absorption spectra of Mn(III)corroles **3a–3c** in CH_2Cl_2

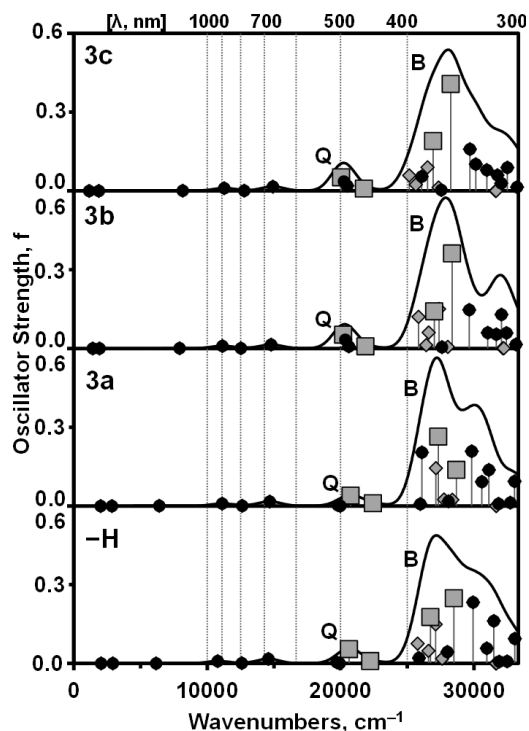


Fig. 4. The TD-DFT calculations for **3a–3c** and a model complex with a phenyl ring at the B *meso*-aryl position (**–H**). Large gray squares are used to highlight the Q and B bands, while black circles are used to denote transitions that are associated with the 3*d* orbitals of the Mn(III) ion. Small gray diamonds are used for transitions associated with the LUMO+1 and LUMO+2 that are localized on the A₂ position *meso*-phenyl rings. The simulated spectra were generated with the Chemcraft program with a fixed bandwidth of 2000 cm⁻¹

the weak broader bands to the red that vary significantly in their band centers are probably associated with LMCT transitions, since the gap between the *a/s* and *-a/-s* MOs do not vary significantly in the TD-DFT calculations (Fig. 2). Upon increasing the electron-donating ability of the B position *meso*-substituent to form **3c**, the broader absorption bands extend beyond 800 nm and can be assigned to LMCT transitions possibly due to slight changes in the energies of the occupied frontier MOs (Fig. 2). The *+/-+/-* sign sequence that is observed for the Faraday \mathcal{B}_0 terms that have been assigned to the Q and B transitions in the MCD spectra (Fig. 3 and Table 1) is consistent with what would be expected based on the relative magnitudes of the splittings (Fig. 2) of the *a* and *s* MOs (the Δ HOMO value in Michl's terminology) and the *-a* and *-s* MOs (the Δ LUMO value). Michl [33–36] has demonstrated that a *+/-+/-* sign sequence is observed when Δ LUMO > Δ HOMO as is the case with **3a–3c** (Fig. 2).

Electrochemistry

Cyclic voltammetry (CV) measurements were carried out in *o*-dichlorobenzene (*o*-DCB) containing

0.1 M tetra-*n*-butylammonium perchlorate (TBAP) as a supporting electrolyte (Fig. 5), to provide further information about the electronic structure of synthetic Mn(III)corroles. **3a–3c** have similar electrochemical properties to those that have been reported previously for similar complexes [38]. The first reduction steps of A₂B type metal corrole complexes have been reported to occur at the central metal, and the second at *ca.* 1.0 V involves reduction of the *meso*-nitrophenyl rings, while the first oxidation step forms a [Mn(III)corrole]⁺ π -cation [39]. The HOMO and LUMO of **3a–3c** are predicted to be a corrole π -system and Mn(III) 3*d* orbitals (Fig. 2), respectively, so similar trends in the redox properties are anticipated in this context. When electron-donating and -withdrawing substituents are introduced at the B *meso*-position, there is an increase or decrease in the electron density on the π -conjugation system of the corrole ligand, respectively, and a decrease or increase in the dipole moment of the complex [40, 41]. The cyclic voltammogram for **3a** has a first reversible [Mn(III)corrole]/[Mn(II)corrole]⁻ reduction step at 0.32 V (in *o*-DCB) (Fig. 5), while there is a negative shift of the $E_{1/2}$ values for **3b–3c** to 0.25 V (**3b**) and 0.20 V (**3c**), respectively, when electron-donating substituents are introduced at the B *meso*-position. The trend in the gaps between the first reduction and oxidation steps (Fig. 5) is consistent with the slight red shift of both the Q and B bands that is observed in the spectroscopic characterization and theoretical calculations of **3b** and **3c** (Figs 2–4 and Table 1) which have more pronounced push–pull properties.

ctDNA interaction

Fluorescence studies were used to quantify the interaction between EB-ctDNA and **3a–3c** (Fig. 6), by using the Stern–Volmer static equation, $I_0/I = 1 + K[Q]$, where I_0 is the original intensity of EB-ctDNA compound at 602 nm, I is the fluorescence intensity upon addition of the Mn(III)corrole to the solution, and $[Q]$ is the concentration of **3a–3c** which act as fluorescence quenchers. The quenching constants (K) for **3a–3c** have been found to be $K = 3.49 \times 10^5$, 4.54×10^5 , and 4.58×10^5 L · mol⁻¹ for **3a–3c**, respectively. The binding ability between ctDNA and Mn(III)corroles increases with the electron donating ability of the *meso*-substituent at the B *meso*-position. There are three possible reasons for the observed fluorescence decrease. Firstly, the formation of a chemical bonded Mn(III)-EB complex causes fluorescence quenching; secondly, Mn(III)corrole binding with EB-ctDNA forms a new non-fluorescent EB-ctDNA-Mn(III)corrole complex, which decreased the fluorescence intensity of EB-ctDNA; and thirdly, the Mn(III)corrole competes with EB in binding with DNA and the intercalated EB was excluded from the DNA double helix, resulting in decreases in the observed fluorescence intensity. These results are noteworthy

Table 1. TD-DFT spectra of **3a–3c** and a model complex with a phenyl ring the B *meso*-aryl position (**–H**) with the CAM-B3LYP functional and 6-31G(d) basis sets

Band ^a	# ^b	Calc ^c			Exp ^d		Wave Function ^e =
3a							
—	1	—	—	—	—	—	Ground state
Q_x	10	20.7	482	(0.05)	≈16.7	≈600	42% s → -a; 27% a → -a; 9% s → L^{dxz}; ...
Q_y	11	22.4	446	(0.01)	17.5	572	42% a → -a; 35% s → -s; ...
B_x	14	27.3	368	(0.19)	23.1	432	50% s → L+1 ^{NO₂} ; 8% a → L+1 ^{NO₂} ; 7% H-4 → L ^{dxz} ; 7% s → -s; 7% s → -a; 6% a → -s; ...
B_y	19	28.7	349	(0.18)	25.0	400	27% a → -s; 26% a → L+1^{NO₂}; 12% a → L+4^{dz²}; 8% s → -a; ...
3b							
—	1	—	—	—	—	—	Ground state
Q_x	8	20.2	495	(0.07)	≈16.7	≈600	28% s → -a; 14% a → -a; 13% s → -s; 10% a → L^{dxz}; 6% s → L^{dxz}; ...
Q_y	11	21.9	457	(0.01)	17.4	576	40% a → L ^{dxz} ; 15% a → -a; 12% a → L^{dxz}; 10% s → -s; ...
B_x	15	27.0	370	(0.18)	23.2	431	18% s → -s; 17% H-2^{dyz} → L^{dxz}; 15% H-5 → L^{dxz}; 10% H-2^{dyz} → a; 8% a → L+2^{NO₂}; ...
B_y	19	28.4	352	(0.48)	25.3	395	47% a → -s; 16% s → -a; 10% a → L+1^{NO₂}; ...
3c							
—	1	—	—	—	—	—	Ground state
Q_x	8	20.1	499	(0.07)	16.8	594	31% s → -a; 14% a → -a; 11% a → L^{dxz}; 11% s → -s; 7% s → L+4^{dz²}; 6% s → L^{dxz}; ...
Q_y	11	21.8	460	(0.01)	≈17.4	≈575	42% a → L+4 ^{dz²} ; 15% a → -a; 12% s → L+4^{dz²}; 10% s → -s; ...
B_x	16	26.9	371	(0.25)	23.5	425	31% s → -s; 16% H-5 → L^{dxz}; 12% a → L+1^{NO₂}; 11% a → L+2^{NO₂}; ...
B_y	19	28.3	354	(0.54)	25.7	389	50% a → -s; 12% s → -a; 8% s → -s; ...
–H							
—	1	—	—	—	—	—	Ground state
Q_x	10	20.6	485	(0.07)	—	—	51% s → -a; 27% a → -s; 11% s → L^{dxz}; ...
Q_y	11	22.2	450	(0.01)	—	—	49% a → -a; 29% s → -s; 8% s → L+4^{dz²}; ...
B_x	15	26.7	374	(0.23)	—	—	23% s → L+2 ^{NO₂} ; 19% a → L+1 ^{NO₂} ; 17% s → -s; 11% H-5 → L^{dxz}; 10% s → L+1^{NO₂}; 5% a → -s; ...
B_y	19	28.5	351	(0.33)	—	—	34% a → -s; 15% H-3^{dx_{xy}} → L+19^{dx²-y²}; 12% s → -a; 7% H-3^{dx_{xy}} → L+23; 6% a → L+1^{NO₂}; ...

a — The band assignment is described in the text. b — Numbers for each state within the TD-DFT calculation are assigned in terms of ascending energy. c — For each calculated spectral band, energies ($10^3 \cdot \text{cm}^{-1}$), wavelengths (nm) and in parentheses oscillator strengths (f) are provided. d — The experimentally observed energies ($10^3 \cdot \text{cm}^{-1}$) and wavelengths (nm) in Fig. 1. e — The wave functions based on the eigenvectors predicted by TD-DFT. Only one-electron transitions that contribute more than 5% are included. Those associated exclusively with the **a**, **s**, **-a** and **-s** MOs of Michl's perimeter model [33–36] are highlighted with bold fonts. NO₂ superscripts are used to denote MOs that are localized on the A₂ position *meso*-aryl rings, while d_{xy}, d_{xz}, d_{yz}, d_{x²-y²} and d_{x²-y²} are used to denote MOs that are primarily associated with the 3d orbitals of the Mn(III) ion.

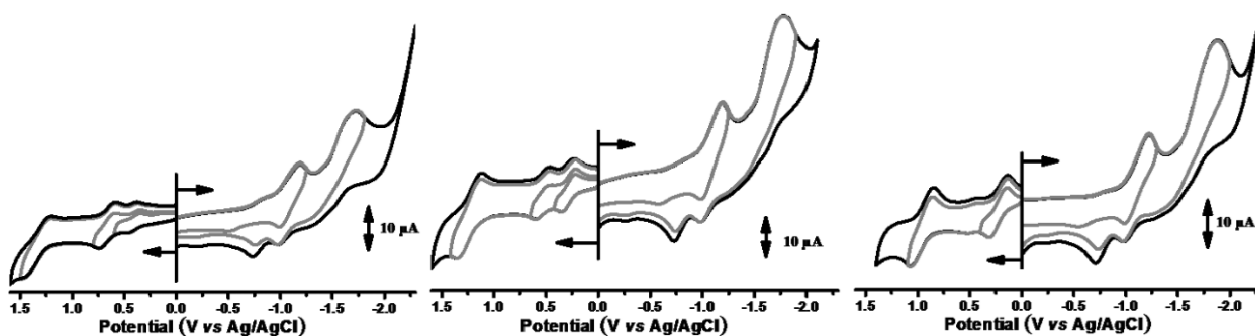


Fig. 5. Cyclic voltammetry measurements of Mn(III)corroles **3a** (left), **3b** (middle) and **3c** (right) in *o*-dichlorobenzene (*o*-DCB)

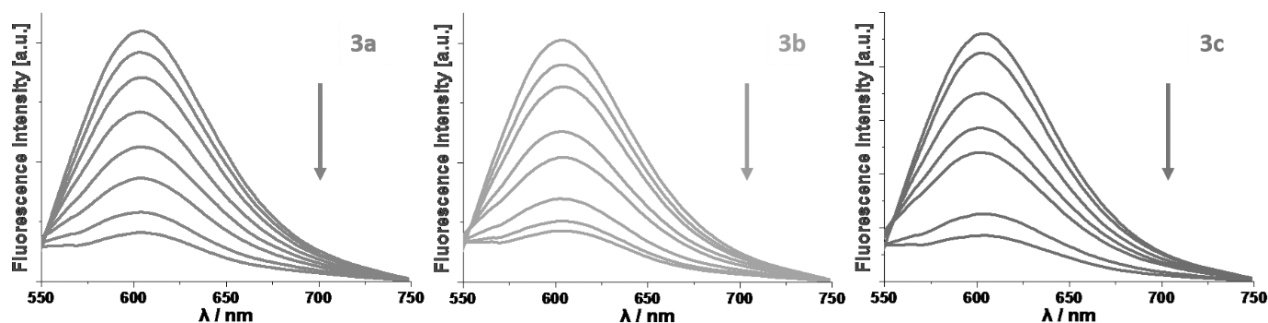


Fig. 6. Fluorescence spectra of EB-ctDNA solution upon addition of Mn(III)corroles **3a–3c**

since they demonstrate that binding with porphyrinoid chromophores with strong intramolecular charge transfer properties could result in less efficient photocleavage by singlet oxygen and hydroxyl radicals.

CONCLUSIONS

A series of Mn(III)triarylcorroles containing asymmetric push-pull *meso*-substitutions have been synthesized and characterized. A detailed analysis of the UV-visible absorption and MCD spectra, cyclic voltammetry measurements, and the results of DFT and TD-DFT calculations has been carried out to identify the key trends in the redox and optical properties. Evidence for normally forbidden LMCT bands associated with the Mn(III) ion was observed in the NIR region of the optical spectra of **3b** and **3c**, which have strong push-pull properties. This study demonstrates that A₂B type Mn(III)triarylcorroles efficiently bond with ctDNA in solution and that the bonding properties can be readily modified by adjusting the push-pull properties of the *meso*-aryl rings.

Acknowledgments

Financial support was provided by the National Scientific Foundation of China (Nos. 21701058, 21571085) and National Scientific Foundation of Jiangsu

province (No. BK20160499), the fund from the state key laboratory of Coordination Chemistry (No. SKLCC1710) and an NRF of South Africa CSUR grant (93627). The theoretical calculations were carried out at the Centre for High Performance Computing in Cape Town.

REFERENCES

- Erben C, Will S and Kadish KM. In *The Porphyrin Handbook*, Vol. 2; Kadish KM, Smith KM and Guillard R, Eds.; Academic Press, Inc.: London, 2000; 232–300.
- Guillard R, Barbe JM, Stern C and Kadish KM. In *The Porphyrin Handbook*, Vol. 18; Kadish KM, Smith KM and Guillard R. Eds.; Academic Press, Inc.: London, 2003; 303–351.
- Liang X, Mack J, Zheng LM, Shen Z and Kobayashi N. *Inorg. Chem.* 2014; **53**: 2797–2802.
- Zhu WH, Huang TT, Qin MF, Li MZ, Mack J and Liang X. *J. Electroanal. Chem.* 2016; **774**: 58–65.
- Li MZ, Niu YJ, Zhu WH, Mack J, Fomo G, Nyokong T and Liang X. *Dyes Pigm.* 2017; **137**: 523–528.
- Niu YJ, Li MZ, Zhang QC, Zhu WH, Mack J, Fomo G, Nyokong T and Liang X. *Dyes Pigm* 2017; **142**: 416–426.
- Isago H and Kagaya Y. *Inorg. Chem.* 2012; **51**: 8447–8454.

8. Simkhovich L, Mahammed A, Goldberg I and Gross Z. *Chem.-Eur. J.* 2001; **7**: 1041–1055.
9. Alcover-Fortuny G, Caballol R, Pierloot K and de Graaf C. *Inorg. Chem.* 2016; **55**: 5274–5280.
10. Liu HY, Yam F, Xie YT, Li XY and Chi CK. *J. Am. Chem. Soc.* 2009; **131**: 12890–12891.
11. Ghosh A. *Chem. Rev.* 2017; **117**: 3798–3881.
12. Liang X, Niu YJ, Zhang QC, Mack J, Yi XY, Hlatshwayo Z, Nyokong T, Li MZ and Zhu WH. *Dalton Trans.* 2017; **46**: 6912–6920.
13. Shimizu S, Haseba Y, Yamazaki M, Kumazawa G and Kobayashi N. *Chem.-Eur. J.* 2014; **20**: 4822–4828.
14. Liang X, Shimizu S and Kobayashi N. *Chem. Commun.* 2014; **50**: 13781–13784.
15. Adam JP and Reich NO. *Biochem.* 2015; **54**: 2181–2192.
16. Witzany G and Baluska F. *EMBO Rep.* 2012; **13**: 1054–1056.
17. Wang LL, Zhang L, Wang H, Zhang Y, Huang JT, Zhu H, Ying X, Ji LN and Liu HY. *J. Phys. Chem. A* 2016; **120**: 535–542.
18. Wang JM, Li Y, Yuan HQ, Wu DH, Ying X, Shi L, Zhang HT and Liu HY. *Appl. Organomet. Chem.* 2017; **31**: e3571–e3583.
19. Shi L, Jiang YY, Jiang T, Yin W, Yang JP, Cao ML, Fang YQ and Liu HY. *Molecules* 2017; **22**: 1084/1-1084/17.
20. Na N, Zhao DQ, Li H, Jiang N, Wen JY and Liu HY. *Molecules* 2016; **21**: 54/1-54/14.
21. Peng SH, Lv BB, Ali A, Wang JM, Ying X, Wang H, Liu JB, Ji LN and Liu HY. *J. Porphyrins Phthalocyanines* 2016; **20**: 624–638.
22. Wang YG, Zhang Z, Wang H and Liu HY. *Bioorg. Chem.* 2016; **67**: 57–63.
23. Piepho SB and Schatz PN. *Group Theory in Spectroscopy With Applications to Magnetic Circular Dichroism*, John Wiley & Sons, Hoboken, NJ, 1983.
24. Kobayashi N, Muranaka A and Mack J. *Circular Dichroism and Magnetic Circular Dichroism Spectroscopy for Organic Chemists*, Royal Society of Chemistry, Cambridge, 2011.
25. Mack J. *Chem. Rev.* 2017; **117**: 3444–3478.
26. Gaussian 09, Revision A.02, Frisch MJ, Trucks GW, Schlegel HB, Scuseria GE, Robb MA, Cheeseman JR, Scalmani G, Barone V, Mennucci B, Petersson GA, Nakatsuji H, Caricato M, Li X, Hratchian HP, Izmaylov AF, Bloino J, Zheng G, Sonnenberg JL, Hada M, Ehara M, Toyota K, Fukuda R, Hasegawa J, Ishida M, Nakajima T, Honda Y, Kitao O, Nakai H, Vreven T, Montgomery JA, Jr, Peralta JE, Ogliaro F, Bearpark M, Heyd JJ, Brothers E, Kudin KN, Staroverov VN, Kobayashi R, Normand J, Raghavachari K, Rendell A, Burant JC, Iyengar SS, Tomasi J, Cossi M, Rega N, Millam JM, Klene M, Knox JE, Cross JB, Bakken V, Adamo C, Jaramillo J, Gomperts R, Stratmann RE, Yazyev O, Austin AJ, Cammi R, Pomelli C, Ochterski JW, Martin RL, Morokuma K, Zakrzewski VG, Voth GA, Salvador P, Dannenberg JJ, Dapprich S, Daniels AD, Farkas Ö, Foresman JB, Ortiz JV, Cioslowski J and Fox DJ. Gaussian, Inc., Wallingford CT, 2009.
27. Cai ZL, Crossley MJ, Reimers JR, Kobayashi R and Amos RD. *J. Phys. Chem. B* 2006; **110**: 15624–15632.
28. Mack J, Stone J and Nyokong T. *J. Porphyrins Phthalocyanines* 2014; **18**: 630–641.
29. Chen QY, Fu HJ, Zhu WH, Qi Y, Ma ZP, Zhao KD and Gao J. *Dalton Trans.* 2011; **40**: 4414–4420.
30. Cory M, Mckee DD, Kagan J, Henry DW and Miller JA. *J. Am. Chem. Soc.* 1985; **107**: 2528–2536.
31. Li MZ, Zhu WH, Mack J, Mkhize S, Nyokong T and Liang X. *Chin. J. Struct. Chem.* 2017; **36**: 367–380.
32. Gouterman M. In: D. Dolphin (Ed.), *The Porphyrins*, Vol. III, Part A, Academic Press, New York, 1978, pp. 1–165.
33. Michl J. *J. Am. Chem. Soc.* 1978; **100**: 6801–6811.
34. Michl J. *Pure Appl. Chem.* 1980; **52**: 1459–1469.
35. Michl J. *Tetrahedron* 1984; **40**: 3845–3894.
36. Michl J. *J. Am. Chem. Soc.* 1978; **100**: 6812–6818.
37. Mack J. *Chem. Rev.* 2017; **117**: 3444–3478.
38. Liu HY, Mahmood MHR, Qiu SX and Chang CK. *Coord. Chem. Rev.* 2013; **257**: 1306–1333.
39. Li BH, Ou ZP, Meng DY, Tang JJ, Fang YY, Liu R and Kadish KM. *J. Inorg. Biochem.* 2014; **136**: 130–139.
40. Ghosh A. *Chem. Rev.* 2017; **117**: 3798–3881.
41. Fang YY, Ou ZP and Kadish KM. *Chem. Rev.* 2017; **117**: 3377–3419.